

1 The layer impact of DNA translocation through graphene nanopores

2 *Wenping Lv¹, Maodu Chen², Ren'an Wu^{1*}*

3

4 ¹, CAS Key Lab of Separation Sciences for Analytical Chemistry, National Chromatographic R&A
5 Center, Dalian Institute of Chemical Physics, Chinese Academy of Sciences (CAS), Dalian,
6 116023, China

7 ², School of Physics and Optoelectronic Technology, Dalian University of Technology, Dalian
8 116024, China

9

10 **Received Date**

11 **Corresponding Author Footnotes**

12 Prof. Dr. Ren'an Wu

13 Tel: +086-411-84379828

14 Fax: +86-411-84379617

15 E-mail: wenping@dicp.ac.cn, wurenan@dicp.ac.cn

16

17

18 **Abstract:**

19 Graphene nanopore based sensor devices are exhibiting the great potential for the
20 detection of DNA. To understand the fundamental aspects of DNA translocating
21 through a graphene nanopore, in this work, molecular dynamics (MD) simulations
22 and potential of mean force (PMF) calculations were carried out to investigate the
23 layer impact of small graphene nanopore (2 nm-3 nm) to DNA translocation. It was
24 observed that the ionic conductance was sensitive to graphene layer of
25 open-nanopores, the probability for DNA translocation through graphene nanopore
26 was related with the thickness of graphene nanopores. MD simulations showed that
27 DNA translocation time was most sensitive to the thickness of graphene nanopore
28 for a 2.4 nm aperture, and the observed free energy barrier of PMFs and the profile
29 change revealed the increased retardation of DNA translocation through bilayer
30 graphene nanopore as compared to monolayer graphene nanopore.

31

32 **Keywords:** nanopore, graphene, DNA detection, molecular dynamics simulation

33

34 Introduction

35 Nanopore sequencing has been emerging as a new generation technology for DNA
36 sequencing.¹⁻⁵ A variety of biological, solid-stated and biological solid-state hybrid
37 nanopores have been constructed experimentally and/or computationally.^{3, 6-13}
38 Graphene is a two-dimensional sheet of carbon atoms arranged in a honeycomb
39 lattice, possessing remarkable mechanical, electrical and thermal properties.¹⁴⁻¹⁶ The
40 subnanometer thickness (0.34 nm) of graphene sheet comparable to the spatial
41 interval of DNA nucleotide suggests a promising DNA sequencing technology with a
42 resolution at single-base level, because of the expected one recognition point in
43 graphene nanopore rather than the multiple contacts in other nanopores.¹⁷ The
44 controllable nanosculpting of graphene nanopore as well as nanobridge and nanogap
45 with few-nanometer precision was first demonstrated by Fischbein and Drndić with a
46 focused electron beam.¹⁸ After that, various graphene nanopores were fabricated
47 with apertures around 5-23 nm (subnanometer thick, monolayer or bilayer
48 graphene),¹⁹ 5-10 nm (1-5 nm thick, *ca.* 3-15 monolayer graphene)²⁰ and 2-40 nm
49 (0.3-2.7 nm thick, monolayer to eight-layer graphene)²¹ etc. Subsequently, the
50 translocation of DNA through nanometer and subnanometer thick graphene
51 nanopores was realized experimentally, with current blockade larger than same size
52 traditional solid-state nanopores.¹⁹⁻²¹

53 It is interestingly that Golovchenko and co-workers found that the conductance of
54 a monolayer graphene nanopore was proportional to the aperture of nanopore.¹⁹
55 However, Dekker *et al.* and Schulten *et al.* demonstrated that the pore conductance
56 was proportional to the square of nanopore diameter by means of experiment²¹ and
57 MD simulation²², respectively, similar as the conductance for traditional solid-stat
58 nanopores (e.g. SiN nanopore²³) which are much thicker. Additionally, it displayed
59 that the conductance of graphene nanopores was impacted by the number of
60 graphene layers, such as for given small graphene nanopores of aperture at 5 nm
61 where ,the conductance of monolayer graphene nanopore was higher than
62 multilayer graphene nanopores, but the conductance of four-layer graphene

63 nanopore was lower than five-layer graphene nanopore.²¹ It seemed plausible as
64 terrace effect was observed in multilayer graphene nanopores created by TEM, that
65 the pore edge of multilayer graphene nanopore was much thinner than the layer
66 thickness of the multilayer graphene membrane.²⁴ On the other hand, Drndic *et al.*
67 used a nanopore constructed in multilayer graphene with pore diameter similar as
68 Golovchenko which gave deeper DNA-induced current blockade than nanopores in
69 monolayer graphene.²⁰ Though these intriguing differences between monolayer
70 graphene nanopores and multilayer graphene nanopores have been observed, the
71 effect of the thickness of graphene nanopore edge to open-pore conductance and
72 translocation of DNA is still unclear.

73 By means of the numerical simulation of solving Poisson–Nerst–Planck equation
74 with COMSOL Multiphysics finite element solver, Garaji *et al.* suggested that the
75 graphene monolayer with a 2.4 nm nanopore has the capability to probe DNA
76 molecule (though be modeled as a stiff insulating rod) with a spatial resolution of
77 0.35 nm (comparable to the distance between two base-pairs in duplex-DNA) at a
78 low translocation speed.¹⁹ In addition, the translocation of DNA through protein and
79 solid-state nanopores have also been successfully investigated by MD simulations at
80 atomic level.²⁵⁻²⁸ An all-atom MD simulation was recently carried out to investigate
81 the microscopic kinetics of DNA translocation through graphene nanopore, and the
82 strong effect of external voltage and DNA conformation on ionic current blockade
83 was observed, consistent with experimental observations.²² Moreover, the
84 discrimination ability of monolayer graphene nanopores to A-T and G-C base pairs
85 (bp) has also been suggested.²² More recently, researchers found that ionic current
86 blockades produced by different DNA nucleotides were, in general, indicative of the
87 nucleotide type, although very sensitive to the orientation of the nucleotides in the
88 nanopore.²⁹ These findings allow researcher one step closer to DNA sequencing using
89 graphene nanopores.

90 Herein, the all-atom MD simulation and potential of mean force (PMF) calculation
91 were carried out to investigate the thickness impact of graphene nanopore toward
92 the pore conductance and DNA translocation. As the terraced effect of multilayer

93 graphene nanopore was observed,²⁴ in this work, graphene nanopores with
94 subnanometer thickness constructed in monolayer, bilayer and trilayer graphene
95 were applied for MD simulations to investigate the layer impact of graphene
96 nanopores to pore conductance and DNA translocation. We found that 1) the
97 open-pore ionic conductance could be modulated by the layer and aperture of
98 graphene nanopores; 2) DNA translocation could be retard by a thicker and narrower
99 graphene nanopore; 3) the velocity of DNA translocation was sensitive to the layer of
100 graphene nanopores for aperture at 2.4 nm; 4) the free energy barrier (PMF) of DNA
101 fragment through graphene nanopore was increased with the increase of graphene
102 layer.

103

104 **Simulation details and Methods:**

105 As the demand of single-base spatial resolution of DNA sequencing by graphene
106 nanopore,¹⁹ graphene nanopores with apertures around 2.4 nm were applied. In
107 total, 9 mono-, bi- and trilayer graphene nanopores with apertures of 2 nm, 2.4 nm
108 and 3 nm were constructed for MD simulation. The schematic diagram of MD
109 simulation model and the modeled structure of graphene nanopores were displayed
110 in Figure 1a and 1b, respectively. The performed MD simulation and corresponding
111 parameters were listed in Table S1 (Supporting Information).

112 The open-pore *I-V* curves and ionic conductance of these 9 graphene nanopores at
113 different bias voltages (0 V - 3 V) were estimated. The simulation boxes were
114 dimensioned about 6 x 6 x 10 nm³. The pored graphene sheet was positioned in the
115 middle of water boxes in *X-Y* plan. The ionic concentration was 1M of NaCl. The ionic
116 current $I(t)$ was calculated by²²

$$117 \quad I(t) = \frac{\sum_{i=1}^N q_i [z_i(t+\Delta t) - z_i(t)]}{\Delta t L_z} \quad (1)$$

118 Where, N was the sum runs over all ions, Δt was chosen to be 100 ps, and z_i and
119 q_i were the *Z*-coordinate and the charge of ion i , respectively.

120 The ionic conductance was defined as the reciprocal of ionic resistance²²

$$121 \quad S = \frac{I_{av}}{U_z} \quad (2)$$

122 Where, $U_z = L_z E_z$, L_z and E_z were the length of simulation box and external
123 electric field in Z-direction, respectively. I_{av} was the average of ionic current ($I_{(t)}$)
124 during the last 3 ns from a 4 ns MD simulation.

125 To investigate the thickness effect of graphene nanopores to the translocation of
126 DNA, similar as the simulation for open-pore ionic conductance, the pored graphene
127 sheets are positioned in the middle of three water boxes with dimension of 6 x 6 x 10
128 nm³. Since a long-chain DNA could enter nanopores in configuration of either
129 unfolded or folded,^{19, 30} a short-chain DNA of d-poly(CAGT)₃ (12 base-pairs) was
130 employed in MD simulations and manually put in a position where the head
131 base-pair of DNA was just at the entrance of graphene nanopores (see in Figure 1a).
132 Hundreds of Na⁺ and Cl⁻ ions were added into the simulation system to make the
133 concentration of NaCl at 1 M and electrically neutral. Four bias voltages of 1, 2, 3 and
134 4 V in Z-direction (perpendicular to graphene membrane, see in Figure 1a) were
135 applied to drive DNA chain through nanopores electrophoretically. In sum, 36 MD
136 simulations with different parameters were set up to study the layer impact of
137 graphene nanopore to DNA translocation (see in Table S1 in Supporting Information).

138 To understand the inherent difference of DNA translocation in graphene
139 nanopores with different thickness, PMFs of DNA translocation along the centre line
140 of nanopores was calculated further by means of the umbrella sampling combining
141 with the weighted histogram analysis method (WHAM).³¹⁻³⁴ Since the conformational
142 fluctuation of a long chain DNA was so huge during the translocation through a
143 nanopore, it's impossible to get an effective sampling distribution in acceptable
144 simulation time. Thus a shorter DNA fragment composed with only two base-pairs
145 (ApT and GpC) was built for PMF calculation (see in Figure 1c). Because the
146 orientation DNA in nanopores could impact the interactions between DNA and
147 nanopore, an ideal model that DNA fragment positioned in the center of graphene
148 nanopore was normally employed (Figure 1d).³⁵ The reaction coordinate was defined
149 as the distance between the centre-of-mass of DNA fragment and a graphene
150 nanopore in Z-direction. The length of the calculated reaction coordinate was 1 nm,
151 which could capture both the effects of DNA entrance and translocation in graphene

152 nanopores. In order to ensure the accuracy of PMF calculation, the width of umbrella
153 window was set at 0.1 nm. There were 11 sampling simulations carried out for each
154 PMF calculation, with umbrella potential of

$$155 \quad w_i(\varphi) = k/2 (\varphi - \varphi_i^c)^2 \quad (3)$$

156 Which restrains DNA at the position φ_i^c ($i=0, \dots, 10$). A force constant of
157 $k = 1,000 \text{ kJ}/(\text{mol} \cdot \text{nm}^2)$ was selected to ensure the validity of sampling. Three
158 atoms in each nucleobase (diagrammatized in the insets of Figure 1d) were
159 restrained by a two dimension (2D)-harmonic potential with force constant
160 at $1,000 \text{ kJ}/(\text{mol} \cdot \text{nm}^2)$ in X - and Y -direction.^{36, 37} Thus the undesirable
161 conformations such as the nucleobases stack within base-pair or the pairing broken
162 for base-pairs were excluded in sampling simulations. The umbrella positions were
163 recorded every step during simulations, with a total simulation time of 10 ns for each
164 sampling simulation. More than 200 ns sampling simulations were carried out in total.
165 The `g_wham` program was used to reconstruct the free energy profiles from the
166 umbrella histograms that were collected during umbrella sampling simulations.³¹ The
167 umbrella histograms for monolayer and bilayer graphene nanopores were illustrated
168 in Figure S1 and S2, respectively (Supporting Information).

169 The structures of DNA used in above simulations were all in A-DNA model and
170 built with the program of X3DNA.³⁸ The graphene nanopores were generated by the
171 VMD program.³⁹ All MD simulations were carried out by means of GROMACS 4.5
172 program package.⁴⁰ The AMBER99 force field⁴¹ was used to model DNA segments
173 and TIP3P⁴² water molecules and ions. The parameters for graphene carbon atoms
174 were those of *sp*² carbon in benzene in the AMBER99 force field. A harmonic
175 potential with a force constant of $1,000 \text{ kJ}/(\text{mol} \cdot \text{nm}^2)$ was used to constrain the
176 position of carbon atoms near the boundary (see in Figure 3b).²² The cut-offs of van
177 der Waals (vdW) force were implemented by a switching function starting at a
178 distance of 1.1 nm and reaching to zero at 1.2 nm. The particle mesh Ewald (PME)
179 method was used to calculate the electrostatic interactions with a cut-off distance of
180 1.4 nm.⁴³ Three-dimensional periodic boundary conditions (PBC) were applied in

181 simulations. Time step of 2 fs was set. Each simulation included 1,000 steps energy
182 minimization, 50 ps solvent relaxation, 500 ps equilibration with DNA constraint and
183 the production MD with time duration from 4 ns to 10 ns, depending on the
184 requirements in different simulation sections (the detailed parameters for each
185 simulation segment please see Table S1 in Supporting Information).

186

187 **Results and discussion:**

188 ***I-V* curves and ionic conductance of open graphene nanopores**

189 Ionic conductance is an important parameter to describe the migration of ions
190 through a nanopore under an applied electric field.^{19-21, 44} The open-pore
191 conductance could directly impact the magnitude of ionic current signal. The effect
192 of ion migration on pore resistance has been observed experimentally.⁴⁴ Here the
193 layer effect of graphene nanopores to ionic conductance was investigated.

194 At first, the current response of open-pore to the bias voltage was studied by
195 monitoring the *I-V* curves. The obtained *I-V* curves were shown in Figure 2a for
196 graphene nanopores with different thicknesses (mono-, bi- and trilayer graphene)
197 and apertures (2 nm, 2.4 nm and 3 nm). On the whole, the current response curves
198 were changed with the increase of graphene layers. While the sensitivities of ionic
199 current to the thickness of graphene nanopores were also impacted by nanopore
200 diameter. For example, the current curves of 2nm nanopores on bilayer and trilayer
201 graphene could not be well distinguished until the applied bias voltages were
202 increased to 3V. While the current curves for wider nanopores (2.4 nm and 3 nm
203 apertures) were obviously sensitive to the add-layers of graphene. As shown in
204 Figure 2a, the noise of ionic current (the error bar) was around 1 nA even no bias
205 voltage applied (caused by self-diffusion of ions and the flexibility of graphene
206 nanopores), and increased with the increase of applied bias voltage (up to 3.5 nA for
207 higher bias voltage). It indicated that the current noise was comparable with the
208 interference of add-layers of graphene and seemed not negligible. However, a recent
209 experiment demonstrated that the electrical noise could be effectively reduced by

210 using a nanopore constructed in a graphene- Al_2O_3 nanolaminate membrane.⁴⁵

211 The ionic conductances (Figure 2b) for the nine graphene nanopores were
212 calculated from the linear fitting of I - V curves. The ionic conductances for monolayer
213 graphene nanopores with apertures of 2 nm and 3 nm were about 5 nS and 9 nS,
214 which were consistent with those of experimental and computational
215 measurements.^{19, 22} It can be seen that the open-pore ionic conductances with
216 different apertures were decreased when the layer number of graphene nanopore
217 increased from mono-, bi- to trilayer, respectively (Figure 2b). These results indicate
218 that within small aperture and subnanometer thickness scale, the ionic conductance
219 might be modulated by even adding or deducting a layer of carbon atoms on
220 graphene nanopores.

221

222 **Layer impact of DNA translocation through graphene nanopores**

223 To investigate DNA translocation through graphene nanopores with different layers,
224 similar as previous section, nine graphene nanopores on mono-, bi- and trilayer
225 graphene sheets were constructed, with applied bias voltages ranged from 1 V to 4V.
226 As listed in Table S1, 36 simulation systems were established for the investigation of
227 DNA translocation processes through graphene nanopores. Each DNA translocation
228 simulation was repeated for three times by using different initialization seeds to
229 enhance its reliability.

230 The statistics of DNA translocation events were displayed in Figure 3a. It can be
231 seen that the DNA translocation processes were sensitive to the thickness and
232 aperture of graphene nanopore. As tabled in Figure 3a, symbol “ + ” denotes the
233 event that DNA could pass through nanopores with remaining as the double-strand
234 structure; symbol “ - ” denotes the event that DNA could not pass through nanopores
235 or the double-strand structure of DNA was disintegrated (such as unwinding or
236 unzipping⁴⁶⁻⁴⁸) during the translocation. As shown in Figure 3a, DNA could pass
237 through a wide and thin nanopore even at the lowest bias voltage. With the increase
238 of the thickness of graphene nanopore, the probability of DNA through nanopore
239 was decreased. Namely, DNA could pass through both 3 nm monolayer and bilayer

240 graphene nanopores under all applied bias voltages (1 V ~ 4 V) in all repeated
241 simulations. While, some “ - ” events occurred in the repeated simulations of DNA
242 translocation in the 3 nm trilayer graphene nanopore. On the other hand, the
243 number of “ + ” events were also decreased with the aperture shrink of nanopores.
244 In all repeat MD simulations, DNA could not pass through the 2 nm nanopore
245 constructed neither on mono-, bi- nor trilayer graphene sheet for bias voltage at 1 V.
246 The possible reason could be the compact interaction between narrow graphene
247 nanopore and DNA molecule, which increased the difficulty for DNA to enter into
248 small nanopores (much detail discussion was given in Section S1 of Supporting
249 Information). These results suggested that the probability of DNA pass through a
250 thick and narrow graphene nanopore should be lower than that DNA pass through a
251 thin and broad graphene nanopore.

252 It is well known that the translocation of DNA through nanopores could be
253 accelerated by applying a higher bias voltage. As shown in Figure 3a, most of the
254 events for DNA translocation through nanopores abided such rule. Whereas, the
255 number of events for DNA passing through 2.4 nm bilayer and 3 nm trilayer graphene
256 nanopores were not always increased with the enhanced bias voltages, suggesting a
257 complex process for DNA translocating graphene nanopores with other possible
258 unrealized factors. As shown in some observation (Figure S4a in Supporting
259 Information), the head of DNA chain could be transformed to a bended conformation,
260 seemed to be relaxed and a B-type DNA.⁴⁹ Subsequently, the bended DNA fallen
261 down and blocked the pore entrance under the drive of applied external electrical
262 field ($t=1566$ ps, Figure S4a). Thus, the increase of the applied bias voltage would not
263 only accelerate the translocation of DNA as expected, but also sometimes promote
264 the yawing of the deformed DNA in some extend. By the way, a recently published
265 work also found that a higher bias voltage may also lead to the translocation of
266 single-strand DNA slower by trapping the DNA in a conformation unfavorable for
267 translocation.²⁹ Thus the conformational variations of DNA before entering the pore
268 entrances might be one of the possible reasons to explain above observations (more
269 detailed discussion for DNA translocation failure was presented in Section S2 of

270 Supporting Information).

271 Herein, the translocation time through nanopores were further analyzed for DNA
272 successfully passing through graphene nanopores (noted as “+” events in Figure 3a).
273 The DNA translocation time of T_t was defined as the duration time for DNA segment
274 (12 bp) to pass through a nanopore from its first base-pair (head) to the last
275 base-pair (end). As shown in Figure 3b, the DNA translocation time was strongly
276 dependent on the applied bias voltage, suggesting an important role of the
277 electrophoretic force for DNA translocation. Comparing DNA translocation in
278 different nanopores, it can be observed that the translocation time of DNA could be
279 modulated by the layer and aperture of graphene nanopores. Where, the
280 translocation time for DNA in 2.4 nm graphene nanopores was most sensitive to the
281 layer of nanopores, with the translocation time of DNA significantly increased with
282 the increased layer of graphene nanopore. While, for the compact nanopores
283 (aperture = 2 nm) and/or the loose nanopores (aperture = 3 nm), the discrimination
284 of DNA translocation time for monolayer and bilayer graphene nanopores were
285 relatively weaker. Moreover, the translocation time for DNA through trilayer
286 graphene nanopores were significantly longer than that through the thinner
287 graphene nanopores for these loose nanopores (aperture > 2 nm). These
288 observations indicated that the thickening of graphene nanopore would reduce the
289 translocation velocity of DNA in nanopores. In addition, a recent published research
290 showed that the rate of “single-base steps”-liked translocation of single-strand DNA
291 seemed increased with the layer numbers of graphene from monolayer to trilayer.²⁹
292 These results suggest that modulate the thickness of graphene nanopore might be a
293 potential scheme for DNA sequencing in single-base precision based on graphene
294 nanopores.

295

296 **PMFs of DNA translocation through graphene nanopore**

297 To understand the fundamental mechanism for DNA translocation through
298 graphene nanopores with different thickness, the calculation of PMFs for DNA
299 translocating along the central line of the 2.4 nm monolayer and bilayer graphene

300 nanopores were carried out. The calculation details of PMFs were described in the
301 section of *Simulation details and Methods*. The calculated PMFs and the snapshots of
302 the in-pore states (A_0 , B_0), out-pore states (A_1 , B_1) and the critical intermediate states
303 (A_b , B_t) were presented in Figure 4. Where, the zero point of free energy were chosen
304 as the reaction coordinate at 1 nm (out-pore states). As shown in Figure 4, the free
305 energy difference of DNA fragment translocation into monolayer graphene nanopore
306 (from state A_1 to state A_0) was about 5 kJ/mol (E_1). While the corresponding average
307 interaction energies (Figure S5a, Supporting Information) between graphene and
308 DNA (GRA-DNA) at state A_1 and state A_0 were -2.52 ± 1.06 kJ/mol and -27.08 ± 6.32
309 kJ/mol, respectively. The enhancement of GRA-DNA interaction suggests that the
310 degree of freedom for DNA in nanopores was reduced. In other words, the free
311 energy barrier between states of A_0 and A_1 was mostly attributed to the entropy
312 decrease due to the constraint of graphene nanopore toward DNA. These results
313 agree with the theories of M. Muthukumar.^{50, 51} With the thickening of graphene
314 nanopore, the interactions between graphene and DNA were enhanced (the average
315 GRA-DNA interaction energies for states B_1 and B_0 were -6.22 ± 3.57 kJ/mol and
316 -60.59 ± 6.40 kJ/mol, respectively, Figure S5b in Supporting Information). Thus a
317 higher free energy barrier about 10 kJ/mol (E_2) was observed for the identical DNA in
318 bilayer graphene nanopore with the same aperture. It suggests that the free energy
319 barrier was additionally modulated by interactions between the DNA and the
320 nanopore.^{50, 51} These results indicated that the constraints induced free energy
321 barriers in graphene nanopores were increase with the increased of the thickness of
322 graphene nanopores.

323 Moreover, an obviously free energy trap ($E_{\text{trap}} = -5$ kJ/mol) was observed before
324 DNA move into the 2.4 nm bilayer graphene nanopore. As shown in Figure 5, at the
325 deepest point of energy trap, the DNA was just positioned at the entrance of bilayer
326 graphene nanopore (state B_t). It indicates that the DNA translocation from state B_1 to
327 state B_t was a free energy falling process. The DNA entering the 2.4 nm bilayer
328 graphene nanopore from the pore entrance (from state B_t to state B_0) need to
329 overcome a energy barrier about 15 kJ/mol ($|E_{\text{trap}}| + E_2$). It was obviously higher

330 than the free energy difference between state B_0 and state B_1 ($E_2 = 10$ kJ/mol).
331 Interestingly, no obviously energy trap was presented at the entrance of monolayer
332 graphene nanopore. So the free energy barrier of DNA entering monolayer graphene
333 nanopore from pore entrance has no significant difference to that from the state A_1
334 ($E_1 = 5$ kJ/mol). Figure 5 also show that a free energy decrease was explicitly existed
335 when DNA shifted from state A_b to state A_0 . While the free energy profile was
336 monotonically increased for DNA translocation from bilayer graphene nanopore
337 entrance (state B_t) into the bilayer graphene nanopore (state B_0). These results show
338 that increase the thickness of graphene nanopores could not only enhance the
339 constraint of nanopore to DNA, but also impact the profiles of PMFs of DNA entering
340 the nanopores.

341

342

343 **Conclusions:**

344 A systematic investigation for DNA translocating through graphene nanopores with
345 different layers at subnanometer thickness was carried out by means of molecular
346 dynamics simulation. It was observed by MD simulation that there is the layer impact
347 of graphene nanopores toward DNA translocation and open-pore conductance.
348 Results indicate that within small aperture and subnanometer thickness scale, even
349 add or deduct a layer of carbon atoms on graphene nanopores could impact their
350 open-pore ionic conductance. The study of DNA translocation in graphene nanopores
351 show the probability of DNA pass through a thick and narrow graphene nanopore
352 should lower than that DNA pass through a thin and wide graphene nanopore. Two
353 reasons were proposed for the failed translocation of DNA in nanopores: 1) For the
354 narrow nanopores (aperture = 2 nm), the compact interactions between narrow
355 graphene nanopores and DNA molecules increased the difficulty of DNA entering
356 small nanopores; 2) While for the loose nanopores (aperture > 2 nm), the
357 conformational transform of DNA at pore entrance might induce the failure of DNA
358 translocation. The probabilities of DNA pass through the loose nanopores (aperture >
359 2 nm) were also decreased with the increase of the thickness of nanopores. In the
360 cases of that DNA successfully passed through graphene nanopores, the velocity of
361 DNA translocation in graphene nanopores seemed to be slowed down by adjusting
362 the thickness and aperture of nanopores. The PMFs analysis showed that the free
363 energy differences for DNA in solution and in nanopores were raised with the
364 increase of layer number of graphene nanopores. The rising of the free energy
365 barriers and the profile change of PMFs could be the fundamental reasons of the
366 increase of the DNA translocation time in bilayer graphene nanopores.

367 In summary, we would conclude that the adjustment of the thickness of graphene
368 nanopores in subnanometer scale would evidently impact DNA translocation in
369 graphene nanopores. Therefore, the precise control of the layer number of graphene
370 at the edge of nanopores should be a very important aspect for DNA translocation as
371 for the prospect nanopore analysis for DNA.

372

373 **Acknowledgement:**

374 This work was supported by the National Natural Science Foundation of China (No.
375 21175134), the Knowledge Innovation Program of Dalian Institute of Chemical
376 Physics and the Hundred Talent Program of the Chinese Academy of Sciences to Dr. R.
377 Wu.

378

379 **Supporting information Available:**

380 All performed MD simulations were listed in Table S1. The umbrella histograms of
381 PMFs calculation for monolayer and bilayer 2.4 nm graphene nanopores were shown
382 in Figure S1 and S2, respectively. In Section S1, the potential reasons of DNA
383 translocation failure in compact graphene nanopores (aperture = 2 nm) were
384 discussed. In Section S2, the potential reasons of DNA translocation failure in loose
385 graphene nanopores (aperture > 2 nm) were discussed. In Figure S3, the snapshots of
386 DNA adhered on the surface of 2 nm monolayer graphene nanopores at 1 V bias
387 voltage were showed (a); the snapshots of the disintegration of the double-strand
388 structure of DNA during it try to pass through the 2 nm monolayer graphene
389 nanopore at 2 V bias voltage were showed (b). In Figure S4, the snapshots of DNA
390 falling down on the surface of 2.4 nm bilayer graphene nanopores at 2 V bias voltage
391 were showed (a); the snapshots of the DNA unwinding/unzipping in 2.4 nm graphene
392 nanopore at 3 V bias voltage were showed (b). In Figure S5, the evolutions of the
393 average interaction energies between DNA and monolayer graphene nanopore (a)
394 and bilayer graphene nanopore (b) long their reaction coordinates were showed.

395

- 397 1. D. W. Deamer and D. Branton, *Accounts Chem Res*, 2002, **35**, 817-825.
- 398 2. J. Shendure and H. L. Ji, *Nat Biotechnol*, 2008, **26**, 1135-1145.
- 399 3. D. Branton, D. W. Deamer, A. Marziali, H. Bayley, S. A. Benner, T. Butler, M. Di Ventra, S. Garaj,
400 A. Hibbs, X. H. Huang, S. B. Jovanovich, P. S. Krstic, S. Lindsay, X. S. S. Ling, C. H. Mastrangelo,
401 A. Meller, J. S. Oliver, Y. V. Pershin, J. M. Ramsey, R. Riehn, G. V. Soni, V. Tabard-Cossa, M.
402 Wanunu, M. Wiggin and J. A. Schloss, *Nat Biotechnol*, 2008, **26**, 1146-1153.
- 403 4. D. Fologea, E. Brandin, J. Uplinger, D. Branton and J. Li, *Electrophoresis*, 2007, **28**, 3186-3192.
- 404 5. Y. Lansac, H. Kumar, M. A. Glaser and P. K. Maiti, *Soft Matter*, 2011, **7**, 5898-5907.
- 405 6. C. Dekker, *Nat Nanotechnol*, 2007, **2**, 209-215.
- 406 7. S. W. Kowalczyk, T. R. Blosser and C. Dekker, *Trends Biotechnol*, 2011, **29**, 607-614.
- 407 8. M. Wanunu, S. Bhattacharya, Y. Xie, Y. Tor, A. Aksimentiev and M. Drndic, *ACS nano*, 2011, **5**,
408 9345-9353.
- 409 9. G. Baaken, N. Ankri, A. K. Schuler, J. Ruhe and J. C. Behrends, *ACS nano*, 2011, **5**, 8080-8088.
- 410 10. B. M. Venkatesan and R. Bashir, *Nat Nanotechnol*, 2011, **6**, 615-624.
- 411 11. A. Meller and D. Branton, *Electrophoresis*, 2002, **23**, 2583-2591.
- 412 12. M. Karhanek, J. T. Kemp, N. Pourmand, R. W. Davis and C. D. Webb, *Nano Lett*, 2005, **5**,
413 403-407.
- 414 13. L. J. Steinbock, O. Otto, D. R. Skarstam, S. Jahn, C. Chimerele, J. L. Gornall and U. F. Keyser, *J*
415 *Phys-Condens Mat*, 2010, **22**.
- 416 14. M. J. Allen, V. C. Tung and R. B. Kaner, *Chem Rev*, 2010, **110**, 132-145.
- 417 15. A. K. Geim, *Science*, 2009, **324**, 1530-1534.
- 418 16. C. N. R. Rao, A. K. Sood, K. S. Subrahmanyam and A. Govindaraj, *Angew Chem Int Edit*, 2009,
419 **48**, 7752-7777.
- 420 17. Z. S. Siwy and M. Davenport, *Nat Nanotechnol*, 2010, **5**, 697-698.
- 421 18. M. D. Fischbein and M. Drndic, *Appl Phys Lett*, 2008, **93**.
- 422 19. S. Garaj, W. Hubbard, A. Reina, J. Kong, D. Branton and J. A. Golovchenko, *Nature*, 2010, **467**,
423 190-U173.
- 424 20. C. A. Merchant, K. Healy, M. Wanunu, V. Ray, N. Peterman, J. Bartel, M. D. Fischbein, K. Venta,
425 Z. T. Luo, A. T. C. Johnson and M. Drndic, *Nano Lett*, 2010, **10**, 2915-2921.
- 426 21. G. F. Schneider, S. W. Kowalczyk, V. E. Calado, G. Pandraud, H. W. Zandbergen, L. M. K.
427 Vandersypen and C. Dekker, *Nano Lett*, 2010, **10**, 3163-3167.
- 428 22. C. Sathe, X. Q. Zou, J. P. Leburton and K. Schulten, *ACS nano*, 2011, **5**, 8842-8851.
- 429 23. M. J. Kim, M. Wanunu, D. C. Bell and A. Meller, *Adv Mater*, 2006, **18**, 3149-+.
- 430 24. B. Song, G. F. Schneider, Q. Xu, G. Pandraud, C. Dekker and H. Zandbergen, *Nano Lett*, 2011,
431 **11**, 2247-2250.
- 432 25. A. Aksimentiev and K. Schulten, *Biophysical journal*, 2005, **88**, 3745-3761.
- 433 26. A. Aksimentiev, J. B. Heng, G. Timp and K. Schulten, *Biophysical journal*, 2004, **87**, 2086-2097.
- 434 27. U. Mirsaidov, W. Timp, X. Zou, V. Dimitrov, K. Schulten, A. P. Feinberg and G. Timp, *Biophysical*
435 *journal*, 2009, **96**, L32-L34.
- 436 28. G. W. Slater, C. Holm, M. V. Chubynsky, H. W. de Haan, A. Dube, K. Grass, O. A. Hickey, C.
437 Kingsburry, D. Sean, T. N. Shendruk and L. X. Nhan, *Electrophoresis*, 2009, **30**, 792-818.

- 438 29. D. B. Wells, M. Belkin, J. Comer and A. Aksimentiev, *Nano Lett*, 2012, **12**, 4117-4123.
- 439 30. J. L. Li, M. Gershow, D. Stein, E. Brandin and J. A. Golovchenko, *Nat Mater*, 2003, **2**, 611-615.
- 440 31. J. S. Hub, B. L. de Groot and D. van der Spoel, *Journal of Chemical Theory and Computation*,
441 2010, **6**, 3713-3720.
- 442 32. J. G. Kirkwood, *J Chem Phys*, 1935, **3**, 300-313.
- 443 33. G. M. Torrie and J. P. Valleau, *Chem Phys Lett*, 1974, **28**, 578-581.
- 444 34. S. Kumar, D. Bouzida, R. H. Swendsen, P. A. Kollman and J. M. Rosenberg, *J Comput Chem*,
445 1992, **13**, 1011-1021.
- 446 35. J. Comer and A. Aksimentiev, *J Phys Chem C*, 2012, **116**, 3376-3393.
- 447 36. B. L. de Groot, T. Frigato, V. Helms and H. Grubmuller, *J Mol Biol*, 2003, **333**, 279-293.
- 448 37. O. Beckstein and M. S. P. Sansom, *P Natl Acad Sci USA*, 2003, **100**, 7063-7068.
- 449 38. X. J. Lu and W. K. Olson, *Nucleic acids research*, 2003, **31**, 5108-5121.
- 450 39. W. Humphrey, A. Dalke and K. Schulten, *Journal of molecular graphics*, 1996, **14**, 33-38,
451 27-38.
- 452 40. B. Hess, C. Kutzner, D. van der Spoel and E. Lindahl, *J Chem Theory Comput*, 2008, **4**, 435-447.
- 453 41. W. D. Cornell, P. Cieplak, C. I. Bayly, I. R. Gould, K. M. Merz, D. M. Ferguson, D. C. Spellmeyer, T.
454 Fox, J. W. Caldwell and P. A. Kollman, *J Am Chem Soc*, 1995, **117**, 5179-5197.
- 455 42. W. L. Jorgensen, J. Chandrasekhar, J. D. Madura, R. W. Impey and M. L. Klein, *J Chem Phys*,
456 1983, **79**, 926-935.
- 457 43. U. Essmann, L. Perera, M. L. Berkowitz, T. Darden, H. Lee and L. G. Pedersen, *J Chem Phys*,
458 1995, **103**, 8577-8593.
- 459 44. C. C. Chen, Y. Zhou and L. A. Baker, *ACS nano*, 2011, **5**, 8404-8411.
- 460 45. B. M. Venkatesan, D. Estrada, S. Banerjee, X. Z. Jin, V. E. Dorgan, M. H. Bae, N. R. Aluru, E. Pop
461 and R. Bashir, *ACS nano*, 2012, **6**, 441-450.
- 462 46. K. Healy, *Nanomedicine-Uk*, 2007, **2**, 459-481.
- 463 47. Q. Zhao, J. Comer, V. Dimitrov, S. Yemencioğlu, A. Aksimentiev and G. Timp, *Nucleic Acids Res*,
464 2008, **36**, 1532-1541.
- 465 48. A. F. Sauer-Budge, J. A. Nyamwanda, D. K. Lubensky and D. Branton, *Phys Rev Lett*, 2003, **90**.
- 466 49. X. Zhao and J. K. Johnson, *J Am Chem Soc*, 2007, **129**, 10438-10445.
- 467 50. M. Muthukumar, *J Chem Phys*, 1999, **111**, 10371-10374.
- 468 51. M. Muthukumar, *Phys Rev Lett*, 2001, **86**, 3188-3191.

469

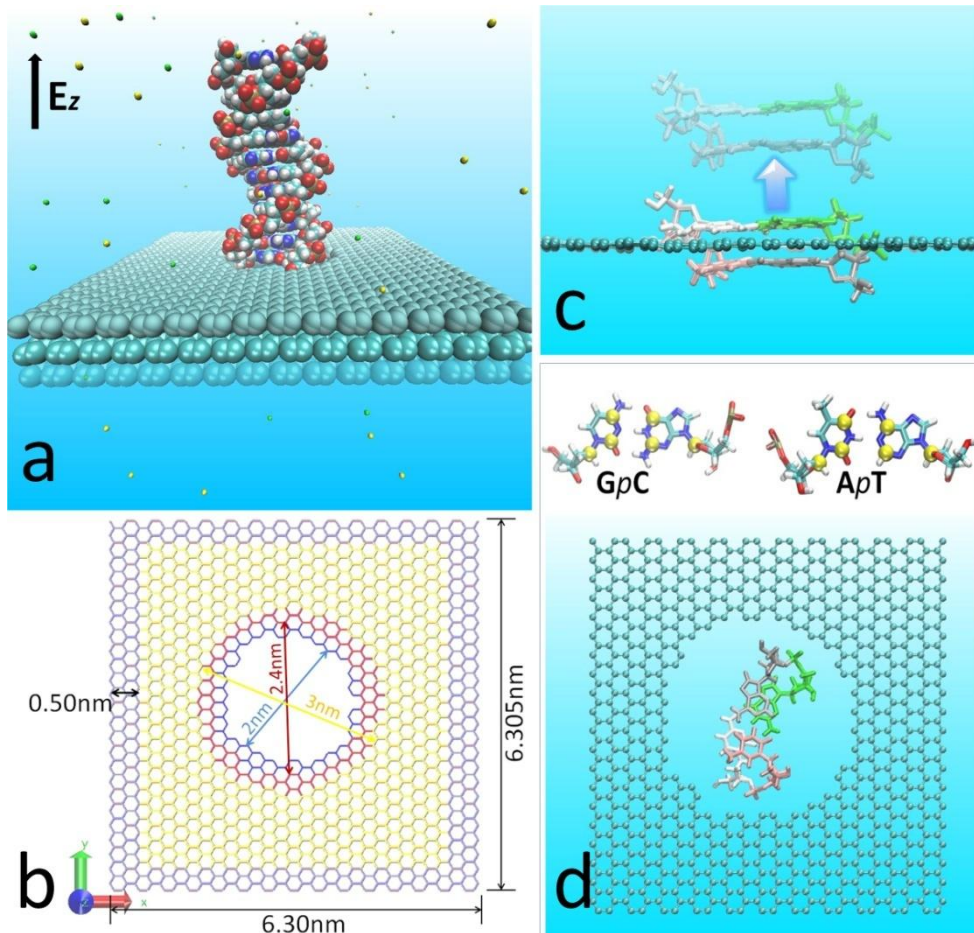
470

471

472

Figures:

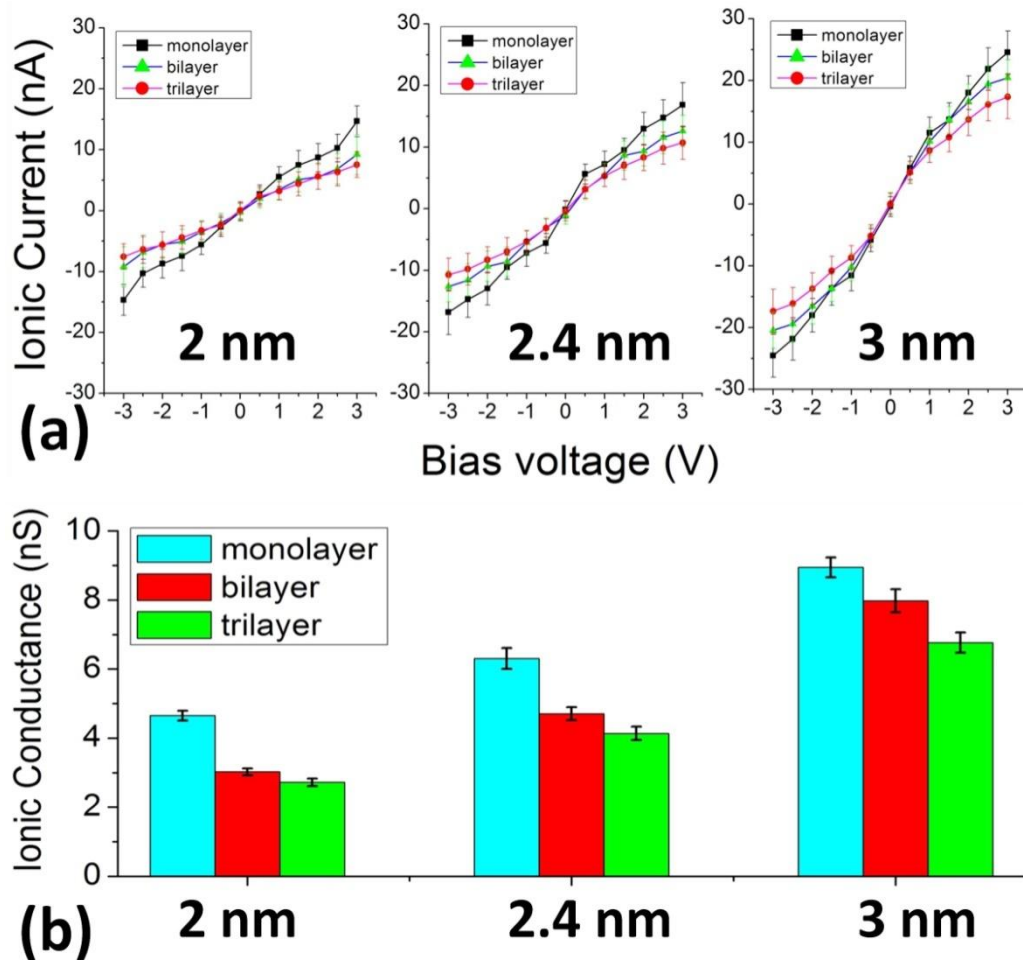
473



474

475 Figure 1. (a) The initial status and scheme of simulation systems for d-poly(CAGT)₃
 476 DNA translocation through trilayer graphene nanopores with aperture of 2.4 nm. The
 477 ions were plotted as small VDW spheres in colors of yellow (Na⁺) and blue (Cl⁻),
 478 respectively. (b) The diagrammatizing of nanopores created on monolayer graphene
 479 sheet with apertures of 2 nm, 2.4 nm and 3 nm. The blue region represents the
 480 restrained atoms. (c) The side view of the in-pore state of DNA and the graphical
 481 representation of the reaction coordinate for PMF calculation (the direction of
 482 arrow). (d) The plan view of the in-pore state of DNA and the graphical
 483 representation of the restrained atoms (shown as yellow balls) in each base-pair.

484



485

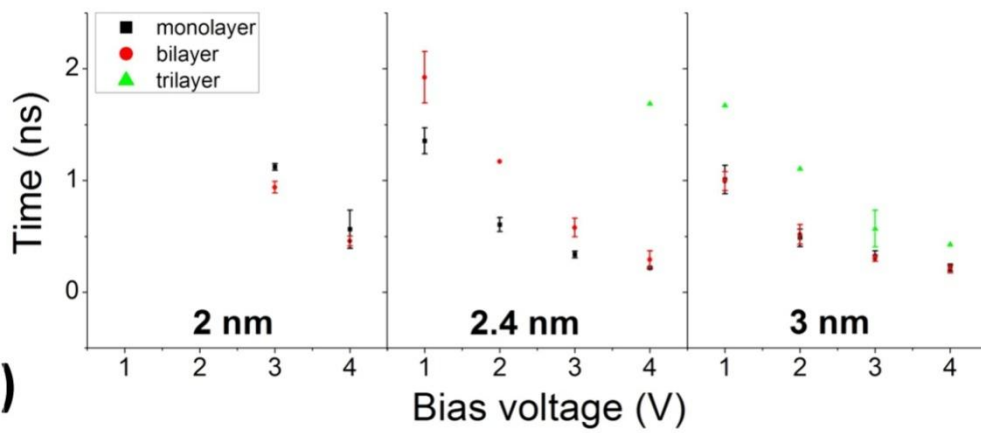
486 Figure 2. (a) I - V curves and (b) ionic conductance for graphene nanopores with
 487 different apertures (2 nm, 2.4 nm and 3 nm) and thicknesses (mono-, bi- and trilayer
 488 graphene). The ionic conductance was obtained by the linear fitting of I - V curves. The
 489 error bars represent the standard deviations.

490

Statistics of DNA translocation events

Aperture (nm)	monolayer			Bilayer			trilayer		
	2	2.4	3	2	2.4	3	2	2.4	3
1 V	---	++-	+++	---	++-	+++	---	---	++-
2 V	+--	+++	+++	---	+--	+++	---	---	++-
3 V	+++	+++	+++	++-	++-	+++	---	+--	+++
4 V	+++	+++	+++	+++	+++	+++	---	+++	++-

(a)



(b)

491

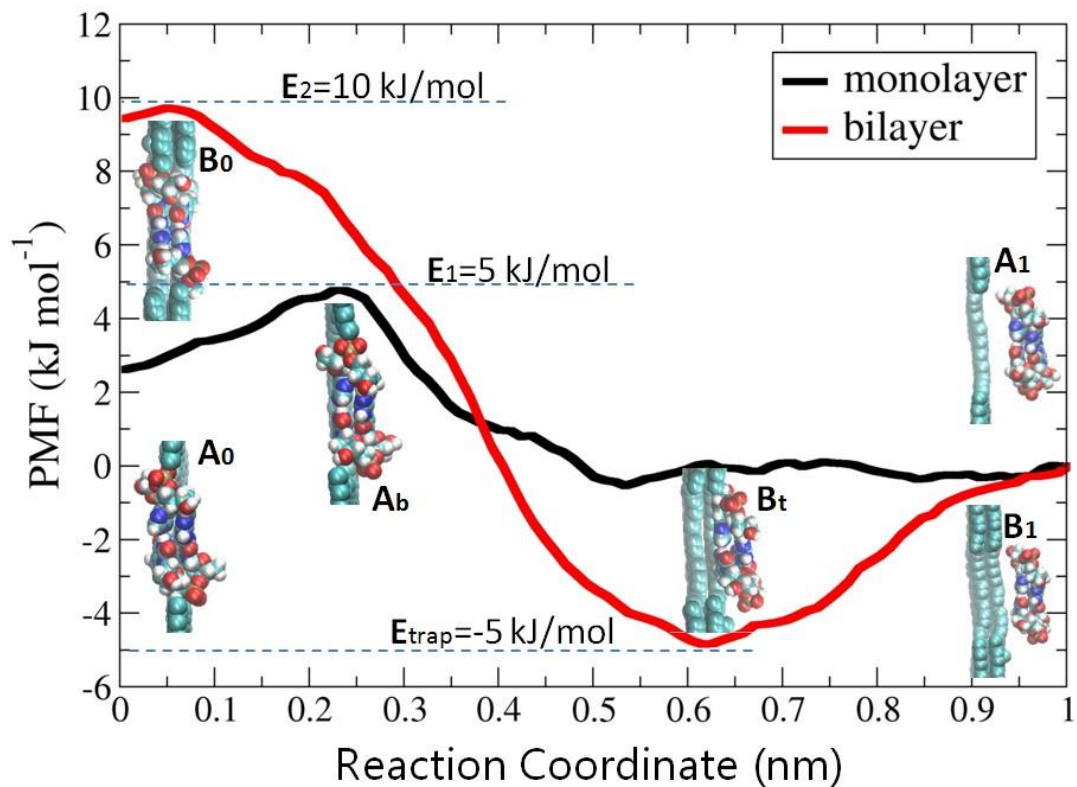
492 Figure 3. (a) The statistics of DNA translocation events with different nanopores.

493 “+” denotes the event that DNA could pass through nanopore; “-” denotes the

494 event that DNA could not pass through nanopore. (b) Translocation time of the

495 events (noted as “+” in Figure 3a) for DNA successfully passing through graphene

496 nanopores.



497

498 Figure 4. PMFs of DNA translocation in monolayer and bilayer graphene nanopores
 499 with aperture of 2.4 nm. The reaction coordinate at 1 nm was chosen as the zero
 500 points of free energy. The in-pore (A_0 , B_0), out-pore (A_1 , B_1) and the critical
 501 intermediate (A_b , B_t) states of DNA translocation through monolayer and bilayer
 502 graphene nanopores were plotted as insets, respectively.

503

504